IEEE Access
Multidisciplinary | Rapid Review | Open Access Journal

Received October 24, 2018, accepted November 9, 2018, date of publication November 14, 2018,
date of current version December 18, 2018.

Digital Object Identifier 10.1109/ACCESS.2018.2881258

Highly Accurate Two-Dimensional Direction Finding Using Cumulant

CHEN GU[1], HONG HONG[1], (Member, IEEE), XIAOHUA ZHU[1], AND JIN HE[2]

[1]School of Electronic and Optical Engineering, Nanjing University of Science and Technology, Nanjing 210094, China
[2]Shanghai Key Laboratory of Intelligent Sensing and Recognition, School of Electronic Information and Electrical Engineering, Shanghai Jiaotong University, Shanghai 200240, China

Corresponding author: Jin He (jinhe@sjtu.edu.cn)

This work was supported by the National Natural Science Foundation of China under Grant 81601568 and Grant 61771302.

ABSTRACT This paper proposes a new two-dimensional direction finding algorithm for estimating multiple non-Gaussian signals using cumulants. This new algorithm: 1) employs an array geometry consisting of a nine-element non-uniformly spaced cross-shaped sub-array plus another arbitrarily-spaced sub-array; 2) defines five cumulant matrices, from which the signal direction cosines can be estimated by using parallel factor fitting, and hence, requiring no open-form two-dimensional searching and parameter pairing; 3) can achieve array aperture extension by jointly extending array physical aperture and constructing virtual sensors, without adding more sensors; and 4) can resolve $2(L-4)$ signals with an array of L sensors in total. Simulation results are presented to verify the efficacy of the proposed algorithm.

INDEX TERMS Array signal processing, direction finding, ESPRIT, parallel factor analysis, cumulant.

I. INTRODUCTION

Estimation of azimuth and elevation arrival angles (two-dimensional directions) of multiple narrowband signals using sensor array techniques has played a fundamental role in many applications involving radar, sonar, wired/wireless communications and seismic sensing. In the past two decades, many efficient one-dimensional direction finding methods, such as MUSIC [1] and ESPRIT [2], are exploited to realize two-dimensional angle estimation [3]–[17]. Among these methods, [3]–[8] consider the MUSIC-type algorithms, and consequently, being computationally ineffective in requiring iterative searching in a two-dimensional domain. References [9]–[14] consider the ESPRIT-type algorithms that avoid searching processes but involve nontrivial pair matching computations between two independent sets of angle estimates (or alteratively two independent sets of direction cosine estimates). References [15]–[17] present the efficient pairing matching methods. The ESPRIT-type algorithms, though have lower computations than MUSIC-type algorithms, they require rotational invariant subarrays, and thus may suffer array aperture losses. Furthermore, all of the above mentioned algorithms require the array inter-sensor spacing within a half-wavelength to guarantee unique and unambiguous angle estimates.

It is well known that an array with larger aperture can offer higher array resolution and more accurate direction-finding precision. Extending array aperture by adding more sensors would increase hardware costs and would add to the computational load required by the signal processors. Extending array aperture by extending the uniform inter-sensor spacing beyond a half-wavelength will lead to a set of cyclically ambiguous direction-cosine estimates, in accordance with the spatial Nyquist sampling theorem. To achieve unambiguous and accurate direction estimates via array aperture extension, we can use a sparse uniform Cartesian-grid array with identical sub-arrays [20]–[25], or to adopt higher order statistics to construct ''virtual sensors'' [26]–[28]. However, most of these approaches require some special constraints in terms of array geometry (e.g., rotational invariant subarrays or sensor locations known *a priori*), and consequently, offer less freedom in the design of the array shape. In this paper, we develop a new algorithm for estimating azimuth-elevation arrival angles of multiple non-Gaussian signals with an array geometry consisting of a nine-element non-uniformly spaced cross-shaped sub-array plus another arbitrarily-spaced sub-array. This new algorithm defines five cumulant matrices, from which the direction cosines of the signal can be estimated by using parallel factor (PARAFAC) fitting [30], and hence, requiring no two-dimensional searching and parameter pairing. This new algorithm can also achieve array aperture extension by jointly extending array physical aperture, which is the effect of the nine-element non-uniformly spaced cross-shaped sub-array), and constructing virtual sensors, which is the effect of the arbitrarily-spaced sub-array,

and hence, can resolve more signals than sensors. Monte Carlo simulation results show that the proposed algorithm can offer distinct performance improvement over the existing techniques in terms of estimation error reduction and less constrained in array geometry.

The rest of this paper is organized as follows. Section II formulates the mathematical data model for the proposed algorithm, Section III develops the proposed algorithm, and Section IV presents the simulation results to demonstrate the efficacy of the proposed algorithm. Section V concludes the paper.

Throughout the paper, scalar quantities are denoted by lowercase letters. Lowercase bold letters are used for vectors, while uppercase bold letters for matrices. Superscripts T, H, $\dagger$ and $*$ represent the transpose, conjugate transpose, pseudo inverse and complex conjugate, respectively.

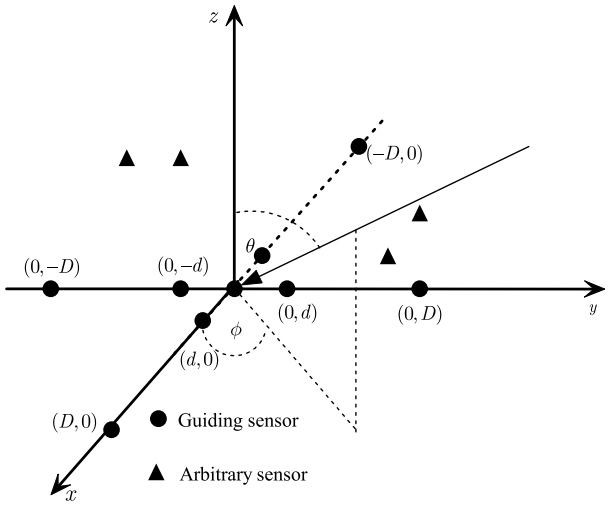

FIGURE 1. Array configuration for the proposed algorithm: a nine-element non-uniformly spaced cross-shaped sub-array plus an arbitrarily-spaced sub-array.

II. DATA MODEL AND ASSUMPTIONS

The present algorithm adopts a L-element array geometry, which consists of a nine-element non-uniformly spaced cross-shaped sub-array plus a $(L-9)$ arbitrarily-spaced sub-array, as shown in Fig. 1. The nine-element non-uniformly spaced cross-shaped sub-array contains sensors located at $(0,0)$, $(\pm d,0)$, $(\pm D,0)$, $(0,\pm d)$ and $(0,\pm D)$ of the $x-y$ plane, whereas the arbitrarily-spaced sub-array contains sensors arbitrarily located in three-dimensional region with possibly unknown locations. The inter-sensor spacing D is assumed to be much larger than a half-wavelength, whereas the spacing d is assumed to be within a half-wavelength. Consider M narrowband non-Gaussian planer wave source signals, parameterized by $\{\theta_1,\phi_1\}$, $\{\theta_2,\phi_2\}$, $\cdots$, $\{\theta_M,\phi_M\}$, impinging upon the array. The parameter $0 \le \theta_m < \pi$ denotes the elevation angle of the mth signal, and $0 \le \phi_m < 2\pi$ represents the azimuth angle of the mth signal.

The data measured by the sensor located at the origin can be expressed as

$$z_0(t) = \sum_{m=1}^{M} s_m(t) + n_0(t) \tag{1}$$

where $s_m(t)$ denotes the complex envelope of the mth signal, $n_0(t)$ represents the additive noise. The 4×1 output vectors measured by the sensors located at $(d,0)$, $(D,0)$, $(0,d)$, $(0,D)$ and $(-d,0)$, $(-D,0)$, $(0,-d)$, $(0,-D)$, respectively, have the complex envelopes represented as

$$\begin{aligned} \boldsymbol{z}_+(t) &= \sum_{m=1}^{M} \boldsymbol{a}_+(\theta_m,\phi_m)s_m(t) + \boldsymbol{n}_+(t) \\ &= \boldsymbol{A}_+\boldsymbol{s}(t) + \boldsymbol{n}_+(t) \end{aligned} \tag{2}$$

$$\begin{aligned} \boldsymbol{z}_-(t) &= \sum_{m=1}^{M} \boldsymbol{a}_-(\theta_m,\phi_m)s_m(t) + \boldsymbol{n}_-(t) \\ &= \boldsymbol{A}_-\boldsymbol{s}(t) + \boldsymbol{n}_-(t) \end{aligned} \tag{3}$$

where $4\times M$ matrices $\boldsymbol{A}_+ = [\boldsymbol{a}_+(\theta_1,\phi_1),\cdots,\boldsymbol{a}_+(\theta_M,\phi_M)]$ and $\boldsymbol{A}_- = [\boldsymbol{a}_-(\theta_1,\phi_1),\cdots,\boldsymbol{a}_-(\theta_M,\phi_M)]$ stand for the array steering matrices, with $\boldsymbol{a}_+(\theta_m,\phi_m) = [e^{j2\pi/\lambda du_m}, e^{j2\pi/\lambda Du_m}, e^{j2\pi/\lambda dv_m}, e^{j2\pi/\lambda Dv_m}]^T$ and $\boldsymbol{a}_-(\theta_m,\phi_m) = [e^{-j2\pi/\lambda du_m}, e^{-j2\pi/\lambda Du_m}, e^{-j2\pi/\lambda dv_m}, e^{-j2\pi/\lambda Dv_m}]^T$, in which $u_m = \sin\theta_m\cos\phi_m$ and $v_m = \sin\theta_m\sin\phi_m$, respectively, signify the direction cosines along the x-axis and y-axis. $\boldsymbol{s}(t) = [s_1(t),\cdots,s_M(t)]^T$ denotes the signal vector. $\boldsymbol{n}_+(t)$ and $\boldsymbol{n}_-(t)$ are 4×1 noise vectors. The $(L-9)\times 1$ array steering vector for the entire $(L-9)$-element arbitrarily-spaced sub-array is

$$\boldsymbol{a}(\theta_m,\phi_m) = [a_1(\theta_m,\phi_m),\cdots,a_{(L-9)}(\theta_m,\phi_m)]^T \tag{4}$$

with $a_\ell(\theta_m,\phi_m) = e^{j2\pi/\lambda(x_\ell u_m + y_\ell v_m + z_\ell w_m)}$ represents the inter-sensor spatial phase factor related to the mth signal and the ℓth sensor at the possibly unknown location (x_ℓ, y_ℓ, z_ℓ), where $w_m = \cos\theta_m$ is the direction cosine along the z-axis. Then, the entire arbitrarily-spaced sub-array would yield the following $(L-9)\times 1$ vector measurement at time t

$$\boldsymbol{z}(t) = \sum_{m=1}^{M} \boldsymbol{a}(\theta_m,\phi_m)s_m(t) + \boldsymbol{n}(t) = \boldsymbol{A}\boldsymbol{s}(t) + \boldsymbol{n}(t) \tag{5}$$

where $\boldsymbol{A} = [\boldsymbol{a}(\theta_1,\phi_1),\cdots,\boldsymbol{a}(\theta_M,\phi_M)]$.

With a total of N snapshots taken at the distinct instants $\{t_n : n = 1,\cdots,N\}$, the problem is to determine the azimuth-elevation arrival angles $\{\theta_m,\phi_m, m=1,\cdots,M\}$ of the impinging signals from these snapshots. We provide a solution to the above-mentioned problem in Section III, under the following assumptions,

i The DOA's $(\theta_1,\phi_1),\cdots,(\theta_M,\phi_M)$ are pairwise distinct, so that the matrix $\boldsymbol{A}$ are of full rank.

ii The impinging signals are zero-mean and stationary, mutually independent, and non-Gaussian, having nonzero fourth-order cumulants.

iii Neither pair of arbitrarily-spaced sensors are symmetric with respect to the origin in the 3D region.

iv The noise is zero-mean, complex Gaussian, and possibly spatially correlated.
v The noise is statistically independent of all the signals.

III. DEVELOPMENT OF THE ALGORITHM

As mentioned above, many existing two-dimentional direction finding algorithms require either two-dimensional searching or pairing of the parameters. In the proposed algorithm, by forming a PARAFAC (PARallel FACtor) model using cumulants, such searching and pairing procedures will be avoided. The PARAFAC analysis is a multi-way method originating from psychometrics [31], [32]. PARAFAC model, as a useful data analysis tool, is a generalization of low-rank matrix decomposition to three-way arrays (TWAs) or multi-way arrays (MWAs). During the past decade, the PARAFAC model is gaining more and more interest in numerous and diverse applications, such as in sensor array signal processing [30] and communications [29]. In the following subsection, we formulate five cumulant matrices, which would be linked to the PARAFAC model in order to recover the directions of the incoming signals.

A. FORMULATION OF THE CUMULANT MATRICES

Let $z_i(t)$, $z_j(t)$, $z_p(t)$, $z_\ell(t)$ be the data measured by the sensors either in the non-uniformly spaced cross-shaped sub-array or in the arbitrarily-spaced sub-array, and let their fourth-order cumulants be $\text{cum}(z_i(t),\ z_j^*(t), z_p(t), z_\ell^*(t))$. Using the assumptions made in last section and cumulant properties given in [33], we have

$$\text{cum}(z_i(t), z_j^*(t), z_p(t), z_\ell^*(t)) = \sum_{m=1}^{M} \gamma_m e^{j2\pi/\lambda(x_{i,j,p,\ell}u_m + y_{i,j,p,\ell}v_m + z_{i,j,p,\ell}w_m)} \quad (6)$$

where

$$\begin{aligned} x_{i,j,p,\ell} &= x_i - x_j + x_p - x_\ell \\ y_{i,j,p,\ell} &= y_i - y_j + y_p - y_\ell \\ z_{i,j,p,\ell} &= z_i - z_j + z_p - z_\ell \end{aligned}$$

with (x_q, y_q, z_q) being the location of the qth sensor, and

$$\gamma_m = \text{cum}(s_m(t), s_m^*(t), s_m(t), s_m^*(t)) = E\{|s_m(t)|^4\} - 2E^2\{|s_m(t)|^2\} - |E\{s_m^2(t)\}|^2 \quad (7)$$

Then, denoting the $(L-4)\times 1$ vector $\bar{\boldsymbol{z}}(t) = [\boldsymbol{z}_0^T(t), \boldsymbol{z}_+^T(t), z^T(t)]^T$ and the $(L-5)\times 1$ vector $\tilde{\boldsymbol{z}}(t) = [\boldsymbol{z}_+^T(t), z^T(t)]^T$, four cumulant matrices are defined as

$$\boldsymbol{R}_{1,1} = \text{cum}(z_0(t), z_0^*(t), \bar{\boldsymbol{z}}(t), \bar{\boldsymbol{z}}^H(t)) = \bar{\boldsymbol{A}}\boldsymbol{\Gamma}\bar{\boldsymbol{A}}^H \quad (8)$$

$$\boldsymbol{R}_{1,2} = \text{cum}(z_0(t), z_0(t), \bar{\boldsymbol{z}}(t), \tilde{\boldsymbol{z}}^T(t)) = \bar{\boldsymbol{A}}\boldsymbol{\Gamma}\tilde{\boldsymbol{A}}^T \quad (9)$$

$$\boldsymbol{R}_{1,3} = \text{cum}(z_0^*(t), z_0^*(t), \tilde{\boldsymbol{z}}^*(t), \bar{\boldsymbol{z}}^H(t)) = \tilde{\boldsymbol{A}}^*\boldsymbol{\Gamma}\bar{\boldsymbol{A}}^H \quad (10)$$

$$\boldsymbol{R}_{1,4} = \text{cum}(z_0(t), z_0^*(t), \tilde{\boldsymbol{z}}^*(t), \tilde{\boldsymbol{z}}^T(t)) = \tilde{\boldsymbol{A}}^*\boldsymbol{\Gamma}\tilde{\boldsymbol{A}}^T \quad (11)$$

where

$$\boldsymbol{\Gamma} = \text{diag}\{\gamma_1, \cdots, \gamma_M\} \quad (12)$$

and $\boldsymbol{R}_{1,1}$, $\boldsymbol{R}_{1,2}$, $\boldsymbol{R}_{1,3}$ and $\boldsymbol{R}_{1,4}$ respectively have dimensions $(L-4)\times(L-4)$, $(L-4)\times(L-5)$, $(L-5)\times(L-4)$ and $(L-5)\times(L-5)$. $\bar{\boldsymbol{A}} = [\bar{\boldsymbol{a}}(\theta_1,\phi_1), \cdots, \bar{\boldsymbol{a}}(\theta_M,\phi_M)]$, with $\bar{\boldsymbol{a}}(\theta_m,\phi_m) = [1, \boldsymbol{a}_+^T(\theta_m,\phi_m), \boldsymbol{a}^T(\theta_m,\phi_m)]^T$ and $\tilde{\boldsymbol{A}}$ is the last $L-5$ rows of $\bar{\boldsymbol{A}}$. Re-arrange $\boldsymbol{R}_{1,1}$, $\boldsymbol{R}_{1,2}$, $\boldsymbol{R}_{1,3}$ and $\boldsymbol{R}_{1,4}$, we can formulate a $(2L-9)\times(2L-9)$ matrix $\boldsymbol{R}_1$ as

$$\boldsymbol{R}_1 = \begin{bmatrix} \boldsymbol{R}_{1,1} & \boldsymbol{R}_{1,2} \\ \boldsymbol{R}_{1,3} & \boldsymbol{R}_{1,4} \end{bmatrix} = \breve{\boldsymbol{A}}\boldsymbol{\Gamma}\breve{\boldsymbol{A}}^H \quad (13)$$

where $\breve{\boldsymbol{A}} = [\bar{\boldsymbol{A}}^T, (\tilde{\boldsymbol{A}}^*)^T]^T$.

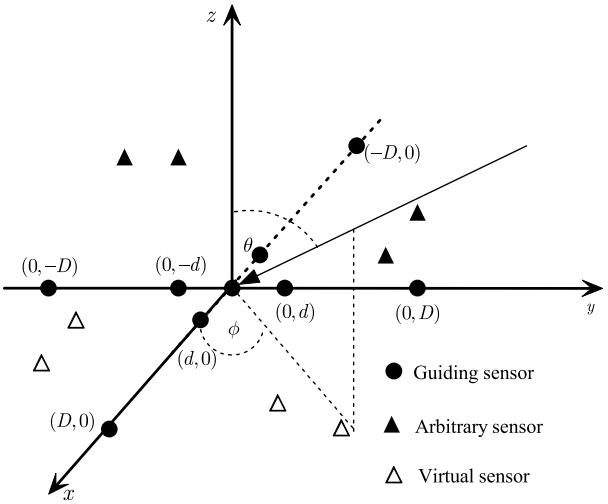

FIGURE 2. Virtual array configuration illustration.

It can be seen from equation (13) that the cumulant matrix $\boldsymbol{R}_1$ would play a similar role as an array covariance matrix, which is from sensors shown in Fig. 2 in the noise-free environment. In (13), $\bar{\boldsymbol{A}}$ in $\breve{\boldsymbol{A}}$ correspond to the physical sensors, which are marked as shaded triangles in Fig. 2, whereas $\tilde{\boldsymbol{A}}^*$ in $\breve{\boldsymbol{A}}$ correspond to the virtual sensors, which are marked as clear triangles in Fig. 2. In other words, the using of the arbitrary sub-array enables the virtual array size extension by forming fourth-order cumulant matrices.

To estimate the signal directions, we further define the following cumulant matrices.

$$\begin{aligned} \boldsymbol{R}_{2,1} &= \text{cum}(z_0(t), z_{+,1}^*(t), \bar{\boldsymbol{z}}(t), \bar{\boldsymbol{z}}^H(t)) \\ &= \bar{\boldsymbol{A}}\boldsymbol{\Phi}_u\boldsymbol{\Gamma}\bar{\boldsymbol{A}}^H \end{aligned} \quad (14)$$

$$\begin{aligned} \boldsymbol{R}_{2,2} &= \text{cum}(z_0(t), z_{-,1}(t), \bar{\boldsymbol{z}}(t), \tilde{\boldsymbol{z}}^T(t)) \\ &= \bar{\boldsymbol{A}}\boldsymbol{\Phi}_u\boldsymbol{\Gamma}\tilde{\boldsymbol{A}}^T \end{aligned} \quad (15)$$

$$\begin{aligned} \boldsymbol{R}_{2,3} &= \text{cum}(z_0^*(t), z_{+,1}^*(t), \tilde{\boldsymbol{z}}^*(t), \bar{\boldsymbol{z}}^H(t)) \\ &= \tilde{\boldsymbol{A}}^*\boldsymbol{\Phi}_u\boldsymbol{\Gamma}\bar{\boldsymbol{A}}^H \end{aligned} \quad (16)$$

$$\begin{aligned} \boldsymbol{R}_{2,4} &= \text{cum}(z_0(t), z_{+,1}^*(t), \tilde{\boldsymbol{z}}^*(t), \tilde{\boldsymbol{z}}^T(t)) \\ &= \tilde{\boldsymbol{A}}^*\boldsymbol{\Phi}_u\boldsymbol{\Gamma}\tilde{\boldsymbol{A}}^T \end{aligned} \quad (17)$$

$$\begin{aligned} \boldsymbol{R}_{3,1} &= \text{cum}(z_0(t), z_{+,2}^*(t), \bar{\boldsymbol{z}}(t), \bar{\boldsymbol{z}}^H(t)) \\ &= \bar{\boldsymbol{A}}\boldsymbol{\Phi}^u\boldsymbol{\Gamma}\bar{\boldsymbol{A}}^H \end{aligned} \quad (18)$$

$$\begin{aligned} \boldsymbol{R}_{3,2} &= \text{cum}(z_0(t), z_{-,2}(t), \bar{\boldsymbol{z}}(t), \tilde{\boldsymbol{z}}^T(t)) \\ &= \bar{\boldsymbol{A}}\boldsymbol{\Phi}^u\boldsymbol{\Gamma}\tilde{\boldsymbol{A}}^T \end{aligned} \quad (19)$$

$$\begin{aligned}\boldsymbol{R}_{3,3} &= \mathrm{cum}(z_0^*(t), z_{+,2}^*(t), \tilde{z}^*(t), \bar{z}^H(t)) \\ &= \tilde{\boldsymbol{A}}^* \boldsymbol{\Phi}^u \boldsymbol{\Gamma} \bar{\boldsymbol{A}}^H \qquad (20)\\ \boldsymbol{R}_{3,4} &= \mathrm{cum}(z_0(t), z_{+,2}^*(t), \tilde{z}^*(t), \tilde{z}^T(t)) \\ &= \tilde{\boldsymbol{A}}^* \boldsymbol{\Phi}^u \boldsymbol{\Gamma} \tilde{\boldsymbol{A}}^T \qquad (21)\\ \boldsymbol{R}_{4,1} &= \mathrm{cum}(z_0(t), z_{+,3}^*(t), \bar{z}(t), \bar{z}^H(t)) \\ &= \bar{\boldsymbol{A}} \boldsymbol{\Phi}_v \boldsymbol{\Gamma} \bar{\boldsymbol{A}}^H \qquad (22)\\ \boldsymbol{R}_{4,2} &= \mathrm{cum}(z_0(t), z_{-,3}(t), \bar{z}(t), \tilde{z}^T(t)) \\ &= \bar{\boldsymbol{A}} \boldsymbol{\Phi}_v \boldsymbol{\Gamma} \tilde{\boldsymbol{A}}^T \qquad (23)\\ \boldsymbol{R}_{4,3} &= \mathrm{cum}(z_0^*(t), z_{+,3}^*(t), \tilde{z}^*(t), \bar{z}^H(t)) \\ &= \tilde{\boldsymbol{A}}^* \boldsymbol{\Phi}_v \boldsymbol{\Gamma} \bar{\boldsymbol{A}}^H \qquad (24)\\ \boldsymbol{R}_{3,4} &= \mathrm{cum}(z_0(t), z_{+,3}^*(t), \tilde{z}^*(t), \tilde{z}^T(t)) \\ &= \tilde{\boldsymbol{A}}^* \boldsymbol{\Phi}_v \boldsymbol{\Gamma} \tilde{\boldsymbol{A}}^T \qquad (25)\\ \boldsymbol{R}_{5,1} &= \mathrm{cum}(z_0(t), z_{+,4}^*(t), \bar{z}(t), \bar{z}^H(t)) \\ &= \bar{\boldsymbol{A}} \boldsymbol{\Phi}^v \boldsymbol{\Gamma} \bar{\boldsymbol{A}}^H \qquad (26)\\ \boldsymbol{R}_{5,2} &= \mathrm{cum}(z_0(t), z_{-,4}(t), \bar{z}(t), \tilde{z}^T(t)) \\ &= \bar{\boldsymbol{A}} \boldsymbol{\Phi}^v \boldsymbol{\Gamma} \tilde{\boldsymbol{A}}^T \qquad (27)\\ \boldsymbol{R}_{5,3} &= \mathrm{cum}(z_0^*(t), z_{+,4}^*(t), \tilde{z}^*(t), \bar{z}^H(t)) \\ &= \tilde{\boldsymbol{A}}^* \boldsymbol{\Phi}^v \boldsymbol{\Gamma} \bar{\boldsymbol{A}}^H \qquad (28)\\ \boldsymbol{R}_{5,4} &= \mathrm{cum}(z_0(t), z_{+,4}^*(t), \tilde{z}^*(t), \tilde{z}^T(t)) \\ &= \tilde{\boldsymbol{A}}^* \boldsymbol{\Phi}^v \boldsymbol{\Gamma} \tilde{\boldsymbol{A}}^T \qquad (29)\end{aligned}$$

where

$$\begin{aligned}\boldsymbol{\Phi}_u &= \mathrm{diag}\{e^{j2\pi/\lambda du_1}, \cdots, e^{j2\pi/\lambda du_M}\} \qquad (30)\\ \boldsymbol{\Phi}^u &= \mathrm{diag}\{e^{j2\pi/\lambda Du_1}, \cdots, e^{j2\pi/\lambda dDu_M}\} \qquad (31)\\ \boldsymbol{\Phi}_v &= \mathrm{diag}\{e^{j2\pi/\lambda dv_1}, \cdots, e^{j2\pi/\lambda dv_M}\} \qquad (32)\\ \boldsymbol{\Phi}^v &= \mathrm{diag}\{e^{j2\pi/\lambda Dv_1}, \cdots, e^{j2\pi/\lambda Dv_M}\} \qquad (33)\end{aligned}$$

Then, similar as $\boldsymbol{R}_1$ is constructed from (8) - (11), we can construct $\boldsymbol{R}_2$, $\boldsymbol{R}_3$, $\boldsymbol{R}_4$ and $\boldsymbol{R}_5$ from (14) - (29) as follows

$$\begin{aligned}\boldsymbol{R}_2 &= \begin{bmatrix}\boldsymbol{R}_{2,1} & \boldsymbol{R}_{2,2}\\ \boldsymbol{R}_{2,3} & \boldsymbol{R}_{2,4}\end{bmatrix} = \breve{\boldsymbol{A}} \boldsymbol{\Phi}_u \boldsymbol{\Gamma} \breve{\boldsymbol{A}}^H \qquad (34)\\ \boldsymbol{R}_3 &= \begin{bmatrix}\boldsymbol{R}_{3,1} & \boldsymbol{R}_{3,2}\\ \boldsymbol{R}_{3,3} & \boldsymbol{R}_{3,4}\end{bmatrix} = \breve{\boldsymbol{A}} \boldsymbol{\Phi}^u \boldsymbol{\Gamma} \breve{\boldsymbol{A}}^H \qquad (35)\\ \boldsymbol{R}_4 &= \begin{bmatrix}\boldsymbol{R}_{4,1} & \boldsymbol{R}_{4,2}\\ \boldsymbol{R}_{4,3} & \boldsymbol{R}_{4,4}\end{bmatrix} = \breve{\boldsymbol{A}} \boldsymbol{\Phi}_v \boldsymbol{\Gamma} \breve{\boldsymbol{A}}^H \qquad (36)\\ \boldsymbol{R}_5 &= \begin{bmatrix}\boldsymbol{R}_{5,1} & \boldsymbol{R}_{5,2}\\ \boldsymbol{R}_{5,3} & \boldsymbol{R}_{5,4}\end{bmatrix} = \breve{\boldsymbol{A}} \boldsymbol{\Phi}^v \boldsymbol{\Gamma} \breve{\boldsymbol{A}}^H \qquad (37)\end{aligned}$$

We refer to the sensors of nine-element non-uniformly spaced cross-shaped sub-array as guiding sensors. More specifically, $z_0(t)$ and $z_0(t)$, $z_0(t)$ and $z_{\pm,1}(t)$, $z_0(t)$ and $z_{\pm,2}(t)$, $z_0(t)$ and $z_{\pm,3}(t)$, $z_0(t)$ and $z_{\pm,4}(t)$ are guiding sensors for constructing $\boldsymbol{R}_1$, $\boldsymbol{R}_2$, $\boldsymbol{R}_3$, $\boldsymbol{R}_4$ and $\boldsymbol{R}_5$, respectively. With the foregoing definitions, we will show in next subsection as to how the matrices $\boldsymbol{R}_1$ - $\boldsymbol{R}_5$ are related to the PARAFAC model.

B. FORMULATION OF THE PARAFAC MODEL

The matrices $\boldsymbol{R}_1$ - $\boldsymbol{R}_5$ can be related to the PARAFAC model as follows. Defining $\boldsymbol{\Upsilon}_1 = \boldsymbol{\Gamma}$, $\boldsymbol{\Upsilon}_2 = \boldsymbol{\Phi}_u \boldsymbol{\Gamma}$, $\boldsymbol{\Upsilon}_3 = \boldsymbol{\Phi}^u \boldsymbol{\Gamma}$, $\boldsymbol{\Upsilon}_4 = \boldsymbol{\Phi}_v \boldsymbol{\Gamma}$, $\boldsymbol{\Upsilon}_5 = \boldsymbol{\Phi}^v \boldsymbol{\Gamma}$, $\boldsymbol{R}_p$ can be re-expressed as $\boldsymbol{R}_p = \breve{\boldsymbol{A}} \boldsymbol{\Upsilon}_p \breve{\boldsymbol{A}}^H$, $p = 1, \cdots, 5$. Stack $\boldsymbol{R}_p$ to form a TWA $\underline{\boldsymbol{R}}$, the (i, p, j)th element of which can be written as

$$r_{i,p,j} = [\underline{\boldsymbol{R}}]_{i,p,j} = \sum_{m=1}^{M} \breve{a}_{i,m} \zeta_{p,m} \breve{a}_{j,m}^* \qquad (38)$$

where $\zeta_{p,m}$ is the mth diagonal element of $\boldsymbol{\Upsilon}_p$. Define a $5 \times M$ matrix $\boldsymbol{G}$ as

$$\boldsymbol{G} = \begin{bmatrix} \gamma_1 & \cdots & \gamma_M \\ \gamma_1 e^{j2\pi/\lambda du_1} & \cdots & \gamma_M e^{j2\pi/\lambda du_M} \\ \gamma_1 e^{j2\pi/\lambda Du_1} & \cdots & \gamma_M e^{j2\pi/\lambda Du_M} \\ \gamma_1 e^{j2\pi/\lambda dv_1} & \cdots & \gamma_M e^{j2\pi/\lambda dv_M} \\ \gamma_1 e^{j2\pi/\lambda Dv_1} & \cdots & \gamma_M e^{j2\pi/\lambda Dv_M} \end{bmatrix} \qquad (39)$$

then $\boldsymbol{\Upsilon}_p$ and $\boldsymbol{G}$ are related by $\boldsymbol{\Upsilon}_p = \mathcal{D}_p(\boldsymbol{G})$.

Equation (38) implies that the cumulant matrices $\boldsymbol{R}_1$ - $\boldsymbol{R}_5$ can be expressed as the low-rank decomposition of the TWA $\underline{\boldsymbol{R}}$, and therefore, the direction finding problem can be reformulated as the problem of low-rank decomposition of the TWA $\underline{\boldsymbol{R}}$, which can be solved by PARAFAC fitting. In fact, we need only to estimate the matrix $\boldsymbol{G}$.

Note that, on the basis of the notion of the Kruskal rank (k-rank) of a matrix, the PARAFAC decomposition of the TWA $\underline{\boldsymbol{R}}$ would be unique under certain conditions. The Kurskal rank (or k-rank) of a matrix $\boldsymbol{A}$ is $k_{\boldsymbol{A}}$, if and only if every $k_{\boldsymbol{A}}$ columns of $\boldsymbol{A}$ are linearly independent and either $\boldsymbol{A}$ has $k_{\boldsymbol{A}}$ columns or $\boldsymbol{A}$ contains a set of $k_{\boldsymbol{A}} + 1$ linearly dependent columns. The Kruskal rank is always less than or equal to the conventional matrix rank. If $\boldsymbol{A}$ is of full column rank, then it is also of full k-rank. From [35], we have if for $M > 1$,

$$k_{\breve{\boldsymbol{A}}} + k_{\boldsymbol{G}} \geq 2M + 2 \qquad (40)$$

then matrices $\breve{\boldsymbol{A}}$ and $\boldsymbol{G}$ are unique up to inherently unresolvable permutation and scaling ambiguities. The uniqueness condition (40) also implies the maximum number of sources that can be identified by the PARAFAC model (38). Using the fact that rank is always less than or equal to the matrix rank, (40) becomes

$$2\min\{2L - 9, M\} + \min\{5, M\} \geq 2M + 2 \qquad (41)$$

Therefore, the trilinear decomposition (38) is unique for any $M \leq 2L - 9$. For $M \geq 2L - 9$, it is unique for $M \leq 2(L - 4)$. These conditions are sufficient for essential uniqueness, but are not always necessary. The above analysis indicates that the proposed algorithm can resolve more sources than sensors. For example, for $L = 11$, the maximum number of sources that can be resolved by the proposed algorithm is $M = 14$.

C. ESTIMATION OF THE DIRECTION COSINES

There exist several effective algorithms that can be used to solve the PARAFAC fitting of $\underline{\boldsymbol{R}}$. The trilinear alternating least square (TALS) algorithm [30], which is based on the idea of reducing the optimization problem to smaller sub-problems that are solved iteratively, is adopted here. In TALS, the parameters to be determined are separated into three sets, and by fixing two of them, a least squares cost function that depends only on the third set is first minimized. With the solution of this linear least squares problem, the subsequent stages of the TALS consist of applying the same principle on the other two sets of parameters. The TALS algorithm iterates, changing from one set to the next, until the variation of the loss function or of the parameters is less than a predefined convergence criterion. Since all the steps are optimizations in the least squares sense, the TALS algorithm is guaranteed to converge monotonically.

To formulate the TALS algorithm mathematically, we define the "slice" matrices of $\underline{\boldsymbol{R}}$ as

$$\boldsymbol{R}_p = [r_{:,p,:}], \quad \boldsymbol{R}'_i = [r_{i,:,:}], \ \boldsymbol{R}''_j = [r_{:,:,j}] \tag{42}$$

where $i, j = 1, \cdots, 2L-9$, $p = 1, \cdots, 5$. For the sake of convenience, let $\boldsymbol{B} = \breve{\boldsymbol{A}}^H$, then, stack $\boldsymbol{R}_p$ for $p = 1, \cdots, 5$, we get the matrix

$$\begin{aligned}\boldsymbol{R} &= \begin{bmatrix}\boldsymbol{R}_1\\ \boldsymbol{R}_2\\ \boldsymbol{R}_3\\ \boldsymbol{R}_4\\ \boldsymbol{R}_5\end{bmatrix} = \begin{bmatrix}\breve{\boldsymbol{A}}\mathcal{D}_1(\boldsymbol{G})\boldsymbol{B}\\ \breve{\boldsymbol{A}}\mathcal{D}_2(\boldsymbol{G})\boldsymbol{B}\\ \breve{\boldsymbol{A}}\mathcal{D}_3(\boldsymbol{G})\boldsymbol{B}\\ \breve{\boldsymbol{A}}\mathcal{D}_4(\boldsymbol{G})\boldsymbol{B}\\ \breve{\boldsymbol{A}}\mathcal{D}_5(\boldsymbol{G})\boldsymbol{B}\end{bmatrix}\\ &= \begin{bmatrix}\breve{\boldsymbol{A}}\mathcal{D}_1(\boldsymbol{G})\\ \breve{\boldsymbol{A}}\mathcal{D}_2(\boldsymbol{G})\\ \breve{\boldsymbol{A}}\mathcal{D}_3(\boldsymbol{G})\\ \breve{\boldsymbol{A}}\mathcal{D}_4(\boldsymbol{G})\\ \breve{\boldsymbol{A}}\mathcal{D}_5(\boldsymbol{G})\end{bmatrix}\boldsymbol{B} = (\boldsymbol{G}\odot\breve{\boldsymbol{A}})\boldsymbol{B}\end{aligned} \tag{43}$$

where $\odot$ is the Khatri-Rao (column-wise Kronecker) matrix product. In the same way, we can have

$$\boldsymbol{R}' = \begin{bmatrix}\boldsymbol{R}'_1\\ \boldsymbol{R}'_2\\ \vdots\\ \boldsymbol{R}'_{2L-9}\end{bmatrix} = (\breve{\boldsymbol{A}}\odot\boldsymbol{B}^T)\boldsymbol{G}^T \tag{44}$$

and

$$\boldsymbol{R}'' = \begin{bmatrix}\boldsymbol{R}''_1\\ \boldsymbol{R}''_2\\ \vdots\\ \boldsymbol{R}''_{2L-9}\end{bmatrix} = (\boldsymbol{B}^T\odot\boldsymbol{G})\breve{\boldsymbol{A}}^T \tag{45}$$

In practice, the exact cumulant matrices $\boldsymbol{R}$, $\boldsymbol{R}'$ and $\boldsymbol{R}''$ are unavailable but can be estimated from sample data. Denote $\hat{\boldsymbol{R}}$, $\hat{\boldsymbol{R}}'$ and $\hat{\boldsymbol{R}}''$ as the estimates of $\boldsymbol{R}$, $\boldsymbol{R}'$ and $\boldsymbol{R}''$, then, the TALS fitting for (43) - (45) is to iteratively minimize the following three equations

$$\min_{\breve{\boldsymbol{A}},\boldsymbol{G},\boldsymbol{B}} = \|\hat{\boldsymbol{R}} - (\boldsymbol{G}\odot\breve{\boldsymbol{A}})\boldsymbol{B}\|_F \tag{46}$$

$$\min_{\breve{\boldsymbol{A}},\boldsymbol{G},\boldsymbol{B}} = \|\hat{\boldsymbol{R}}' - (\breve{\boldsymbol{A}}\odot\boldsymbol{B}^T)\boldsymbol{G}^T\|_F \tag{47}$$

$$\min_{\breve{\boldsymbol{A}},\boldsymbol{G},\boldsymbol{B}} = \|\hat{\boldsymbol{R}}'' - (\boldsymbol{B}^T\odot\boldsymbol{G})\breve{\boldsymbol{A}}^T\|_F \tag{48}$$

where $\|\cdot\|_F$ denotes the Frobenius norm. For each equation, one component matrix is updated in each iteration by fixing the other two to their values obtained from the other two equations. It follows from (46) - (48) that the conditional least square updates of $\boldsymbol{B}$, $\boldsymbol{G}$ and $\breve{\boldsymbol{A}}$ at the rth iteration are given by

$$\hat{\boldsymbol{B}}_r = (\hat{\boldsymbol{G}}_{r-1}\odot\hat{\breve{\boldsymbol{A}}}_{r-1})^\dagger\hat{\boldsymbol{R}} \tag{49}$$

$$\hat{\boldsymbol{G}}_r^T = (\hat{\breve{\boldsymbol{A}}}_{r-1}\odot\hat{\boldsymbol{B}}_{r-1}^T)^\dagger\hat{\boldsymbol{R}}' \tag{50}$$

$$\hat{\breve{\boldsymbol{A}}}_r^T = (\hat{\boldsymbol{B}}_{r-1}^T\odot\hat{\boldsymbol{G}}_{r-1})^\dagger\hat{\boldsymbol{R}}'' \tag{51}$$

To initiate the iteration at $r = 1$, $\hat{\boldsymbol{G}}_0$ and $\hat{\breve{\boldsymbol{A}}}_0$ can be randomly generated. Let $e(r) = \|\hat{\boldsymbol{R}} - (\hat{\boldsymbol{G}}_r\odot\hat{\breve{\boldsymbol{A}}}_r)\hat{\boldsymbol{B}}_r^T\|_F$. Then, the algorithm converges when $|e(r) - e(r-1)| \le \epsilon$, where ϵ is an arbitrarily preset small number.

Since $d \le \lambda/2$ and $-1 \le u_m, v_m \le 1$, then with the estimation of $\hat{\boldsymbol{G}}$, a set of unambiguous but high-variance reference estimates of direction cosines along x-axis and y-axis $(\hat{u}_m^{\text{ref}}, \hat{v}_m^{\text{ref}})$, $m = 1, \cdots, M$ can be derived as

$$\hat{u}_m^{\text{ref}} = \frac{\arg(\hat{g}_{m,2}/\hat{g}_{m,1})}{2\pi d/\lambda} \tag{52}$$

$$\hat{v}_m^{\text{ref}} = \frac{\arg(\hat{g}_{m,4}/\hat{g}_{m,1})}{2\pi d/\lambda} \tag{53}$$

where $\hat{g}_{m,j}, j = 1, \cdots, 5$ denotes the jth element of the mth column of matrix $\hat{\boldsymbol{G}}$. Furthermore, as $D > \lambda/2$, a set of low-variance but cyclically ambiguous direction cosines estimates along x-axis and y-axis $(\hat{u}_m(n_x), \hat{v}_m(n_y))$, $m = 1, \cdots, M$ can also be derived from $\hat{\boldsymbol{G}}$ as

$$\hat{u}_m(n_x) = \mu_m + n_x\frac{\lambda}{D} \tag{54}$$

$$\left\lceil\frac{D}{\lambda}(-0.5-\mu_m)\right\rceil \le n_x \le \left\lfloor\frac{D}{\lambda}(0.5-\mu_m)\right\rfloor \tag{55}$$

$$\mu_m = \frac{\arg(\hat{g}_{m,3}/\hat{g}_{m,1})}{2\pi D/\lambda} \tag{56}$$

$$\hat{v}_m(n_y) = \nu_m + n_y\frac{\lambda}{D} \tag{57}$$

$$\left\lceil\frac{D}{\lambda}(-0.5-\nu_m)\right\rceil \le n_y \le \left\lfloor\frac{D}{\lambda}(0.5-\nu_m)\right\rfloor \tag{58}$$

$$\nu_m = \frac{\arg(\hat{g}_{m,5}/\hat{g}_{m,1})}{2\pi D/\lambda} \tag{59}$$

where $\lceil x\rceil$ denotes the smallest integer not less than x, $\lfloor x\rfloor$ represents the largest integer not greater than x, and $\arg\{z\}$ signifies the principal argument of the complex number z between $-\pi$ and π.

Finally, the reference direction cosines estimates $(\hat{u}_m^{\text{ref}}, \hat{v}_m^{\text{ref}})$, $m = 1, \cdots, M$ are used to resolve the cyclically ambiguous

direction cosines estimates $(\hat{u}_m(n_x), \hat{v}_m(n_y))$, $m = 1, \cdots, M$. The disambiguated x-axis and y-axis direction cosines $\hat{u}_m$ and $\hat{v}_m$ are found from $\hat{u}_m(n_x)$ and $\hat{v}_m(n_y)$ when the value of $|\hat{u}_m(n_x) - \hat{u}_m^{\text{ref}}|$ and $|\hat{v}_m(n_y) - \hat{v}_m^{\text{ref}}|$ are minimized. Mathematically, the disambiguated x-axis direction cosines estimates $\hat{u}_m$ are given by

$$\hat{u}_m = \mu_m + n_x^o \frac{\lambda}{D} \tag{60}$$

where n_x^o is estimated as

$$n_x^o = \underset{n_x}{\text{argmin}} \left| \hat{u}_m^{\text{ref}} - \mu_m - \frac{n_x \lambda}{D} \right| \tag{61}$$

Analogously, the disambiguated y-axis direction cosines estimates $\hat{v}_m$ are given by

$$\hat{v}_m = \nu_m + n_y^o \frac{\lambda}{D} \tag{62}$$

where n_y^o is estimated as

$$n_y^o = \underset{n_y}{\text{argmin}} \left| \hat{v}_m^{\text{ref}} - \nu_m - \frac{n_y \lambda}{\Delta_y} \right| \tag{63}$$

Note that n_x^o and n_y^o are determined separately. The search ranges for n_x^o and n_y^o are given by (55) and (58), respectively, and for each of n_x^o and n_y^o, up to a maximum of $\lfloor 2(D/\lambda) + 1 \rfloor$ candidates are tested.

From the foregoing analysis, the 2D directions of the mth signal can be estimated as

$$\hat{\theta}_m = \arcsin\left(\sqrt{\hat{u}_m^2 + \hat{v}_m^2}\right) \tag{64}$$

$$\hat{\phi}_m = \angle(\hat{u}_m + j\hat{v}_m) \tag{65}$$

D. COMPUTATIONAL COMPLEXITY COMPARISON

In this subsection, we analyze the computational complexities of the proposed algorithm. Four other algorithms are considered here for comparison. We consider the major computations (multiplications) involved in the algorithms. The labels "Cumulant-PARAFAC", "Cumulant-ESPRIT", "Dual-Inv-ESPRIT", "L-Shape-ESPRIT", "Parallel-Shape-ESPRIT" are used for the proposed algorithm, the algorithm in [26], the algorithm in [21], the algorithm in [10] and the algorithm in [11], respectively. For the "Cumulant-PARAFAC", the major computations are (a): to estimate the cumulant matrices $\boldsymbol{R}_1$ - $\boldsymbol{R}_5$ and (b): to perform trilinear decomposition of $\underline{\boldsymbol{R}}$. The resulting multiplications required are in order of $\mathcal{O}(12N(L-4)^2 + 12N(L-4)^2(L-5)^2 + 12N(L-5)^2)$ for (a) and $\mathcal{O}(M^3 + 5M(2L-9)^2)$ per iteration for (b). For the "Cumulant - ESPRIT", the major computations are to compute three cumulant matrices and to perform eigendecomposition for signal subspace extraction. The computations required are in order of $\mathcal{O}(12NL^2 + L^3)$. For the "Dual-Inv-ESPRIT ", the major computations are to construct a correlation matrix and to perform its eigendecomposition. The multiplications needed are in order of $\mathcal{O}(L^2N + L^3)$. For the "L-Shape-ESPRIT", the major computations are to estimate the signal subspace from array data using linear operations. The multiplications required are in order of $\mathcal{O}(2LNM)$. For the "Parallel-Shape-ESPRIT", the major computations are to estimate the signal subspace using linear operations. The multiplications involved are in order of $\mathcal{O}(3LNM)$.

E. ADVANTAGES OF THE PROPOSED ALGORITHM

Relative to most other two-dimensional direction finding algorithms [3], [4], [21], [26]–[28], the above proposed algorithm has the following advantages

(1) The proposed algorithm imposes less constraint on array shape, in the sense that sensors outside the cross-shaped sub-array can be placed in an arbitrarily-shaped array and the locations of these sensors may be unknown.
(2) It requires no two-dimensional searching.
(3) It requires no parameter pairing procedure.
(4) It achieves array aperture extension by constructing virtual sensors using fourth-order cumulants.
(5) It providesly high accurate and unambiguous angle estimates by exploiting the fact that spatial phase factor is larger than a half-wavelength.
(6) It can resolve more signals than sensors. More exactly, it can resolve $2(L-4)$ signals with an array of L sensors.

It is noted that in [3] and [4] the MUSIC algorithm is adapted to a uniform circular array; these algorithms achieve angle estimates by two-dimensional searching, and hence would only have the advantage (3) listed above. The methods in [10] and [11] apply the ESPRIT-like algorithm to L-shape or parallel shape array geometries; these algorithms recover the signal directions from half-wavelength spatial invariance embedded in the array, and hence only have the advantage (2) listed above. Reference [21] presents a sparse array geometry embedding two spatial invariances to obtain highly accurate and unambiguous angle estimation using the ESPRIT technique. This algorithm has the advantages (2) and (5) listed above. Reference [26] derives an ESPRIT-based algorithm using fourth-order cumulants with arbitrary array geometry. However, this algorithm does not extend the array aperture and hence only have the advantages (1) and (2) listed above. The method in [27] develops a MUSIC-like algorithm that can resolve more signals than sensors using higher order statistics. With prior knowledge of the sensor locations, this algorithm would have the advantages (1), (3), (4) and (6) listed above. Reference [28] proposes a PARAFAC-based algorithm by using a special volume array geometry. However, this algorithm requires the inter-sensor spacing is within a half-wavelength, and hence this algorithm would offer neither advantages (1) nor (5).

IV. SIMULATIONS

Simulation results are presented to demonstrate the efficacy of the proposed algorithm. Unless otherwise stated, the array configuration in Fig. 1 with $L = 15$ elements, i.e., a nine-element non-uniformly spaced cross-shaped sub-array plus a six-element arbitrarily-spaced sub-array, is used. We consider the case of two equal-power narrowband non-Gaussian uncorrelated monochromatic signals

impinging upon the array. There are $N = 200$ snapshots in each independent Monte Carlo trials and 500 independent Monte Carlo trials for each data point. Further the additive white noise is assumed to be complex Gaussian, In all the simulations, the performance metric used is the root mean squared error (RMSE) of first signal.

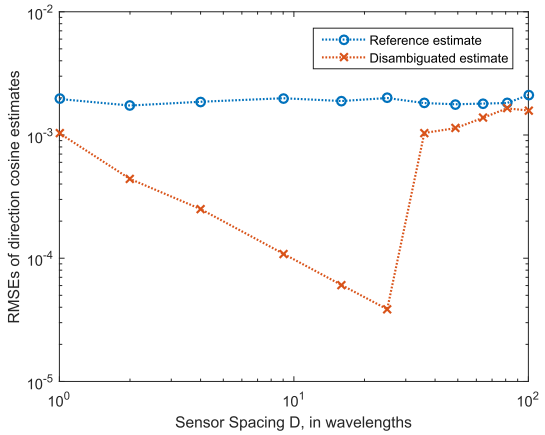

FIGURE 3. RMSEs of the estimates of the direction cosines versus inter-sensor spacing, varying from 1λ to 100λ. Two monochromatic signals with digital frequencies $f_1 = 0.1, f_2 = 0.4$ and direction cosines $u_1 = 0.1, v_1 = 0.2$ and $u_2 = 0.31, v_2 = 0.44$ impinge upon the array.

In the first example, we assess the performance of the proposed algorithm for various values of D, the inter-sensor spacing. Two incident signals arrive with direction cosines $u_1 = 0.1$, $v_1 = 0.2$, $u_2 = 0.31$, $v_2 = 0.44$ are simulated. Fig. 3 shows, on a log-log scale, the RMSEs of the reference direction cosine estimates $(\hat{u}_1^{\text{ref}}, \hat{v}_1^{\text{ref}})$ and disambiguated direction cosine estimates $(\hat{u}_1, \hat{v}_1)$ as a function of D, varying from 1λ to 100λ, λ being the wavelength. The signal-to-noise ratio (SNR) for each of the signals is set 20dB. It is seen that the RMSE of the disambiguated direction cosine estimates decrease linearly as the inter-sensor spacing increases from 1λ up to 25λ. The performance of reference direction cosine estimates remains relatively constant as the inter-sensor spacing increases from 1λ to 100λ. This confirms that the reference direction cosine estimates are high variance but unambiguous. For $D > 36\lambda$, the disambiguated direction cosine estimates have almost the same statistical errors as the reference direction cosine estimates. This behavior is similar to that in [21] and can be explained as follows. Referring to (60) and (62), the estimates $u_1(n_x)$ and $v_1(n_y)$ suffer ambiguities of some unknown integer multiple of the grid size λ/D, respectively. As the inter-sensor spacing D increases, the grid sizes shrink relative to the variances of the reference estimates $\hat{u}_1^{\text{ref}}$ and $\hat{v}_1^{\text{ref}}$. Therefore, it becomes increasingly probable that $\hat{u}_1^{\text{ref}}$ and $\hat{v}_1^{\text{ref}}$ would identify the wrong grid point. As the inter-sensor spacings continue to increase, the grid misidentification will become the dominant error, and the disambiguated estimates $\hat{u}_1$ and $\hat{v}_1$ eventually have the same error statistics as the reference estimates $\hat{u}_1^{\text{ref}}$ and $\hat{v}_1^{\text{ref}}$.

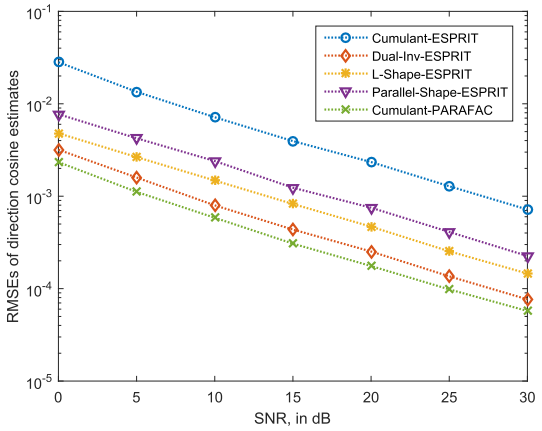

FIGURE 4. RMSEs of the estimates of the direction cosines versus SNR. Two monochromatic signals with digital frequencies $f_1 = 0.1, f_2 = 0.4$ and direction cosines $u_1 = 0.1, v_1 = 0.2$ and $u_2 = 0.31, v_2 = 0.44$ impinge upon the array.

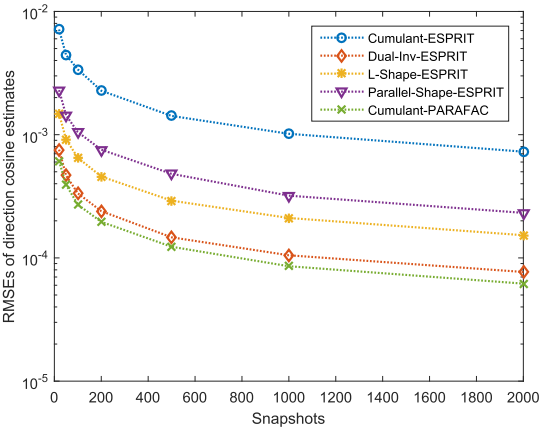

FIGURE 5. RMSEs of the estimates of the direction cosines versus the number of snapshots. Two monochromatic signals with digital frequencies $f_1 = 0.1, f_2 = 0.4$ and direction cosines $u_1 = 0.2, v_1 = 0.4$ and $u_2 = 0.35, v_2 = 0.55$ impinge upon the array.

In the second example, we compare the RMSEs of the proposed algorithm (Cumulant-PARAFAC) with four other subspace-based algorithms using cumulants or other array configurations: the ESPRIT-based algorithm using cumulants (Cumulant-ESPRIT) [26], ESPRIT-based algorithm with dual-size spatial invariance (Dual-Inv-ESPRIT) [21], the ESPRIT-based algorithm using L-shape array (L-Shape-ESPRIT), and the ESPRIT-based algorithm using Parallel-Shape array (Parallel-Shape-ESPRIT). For the Cumulant-ESPRIT algorithm, we assume fifteen-element arbitrarily-spaced array configuration that contains three preset guiding sensors located at $(0, 0)$, $(\lambda/2, 0)$, and $(0, \lambda/2)$. For the Dual-Inv-ESPRIT algorithm, we use a right triangular array grid with spacing D and a five-element half-wavelength spaced cross-shaped sub-array in each grid point. For the four ESPRIT-based algorithms, the estimated sets of direction cosines are assumed to have been correctly paired. In this simulation, the signal direction cosines are taken as $u_1 = 0.2, v_1 = 0.35$ and $u_2 = 0.4, v_2 = 0.55$. For the proposed algorithm and [21], we set $D = 5\lambda$. Figs. 4 and 5,

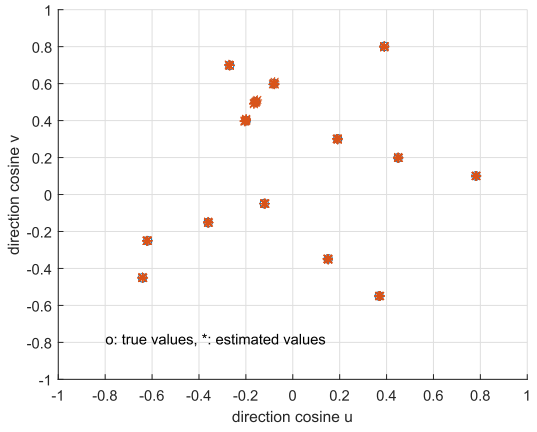

FIGURE 6. Direction-cosine estimates for ten independent trials. $M = 14$ sources with $(u_1, \cdots, u_{14}) = (0.37, -0.64, 0.15, -0.62, -0.36, -0.12, 0.78, 0.45, 0.19, -0.20, -0.16, -0.08, -0.27, 0.39)$ and $(v_1, \cdots, v_{14}) = (-0.55, -0.45, -0.35, -0.25, -0.15, -0.05, 0.1, 0.2, 0.3, 0.4, 0.5, 0.6, 0.7, 0.8)$ impinge upon the array of $L = 11$ sensors.

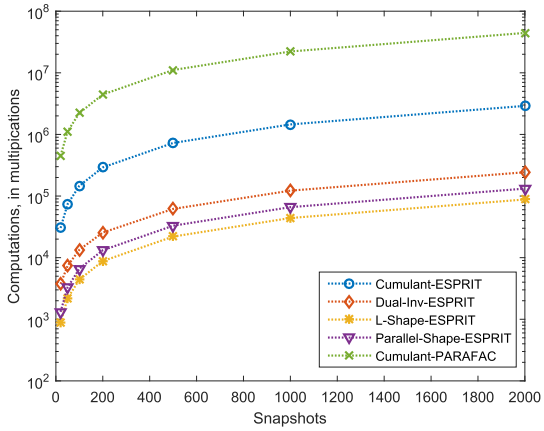

FIGURE 7. Computational costs of the algorithms versus the number of snapshots. $L = 11$, $M = 2$.

respectively show the RMSEs of the five algorithms as a function of SNR, varying from 0dB to 30dB and the number of snapshots, varying from 20 to 2000. The curves in these two figures unanimously indicate that the proposed algorithm has performance superior to its four competitors in term of the lower RMSEs.

In the third example, we show that the proposed algorithm can resolve more sources than sensors. We assume $M = 14$ sources with the following direction-cosines $(u_1, \cdots, u_{14}) = (0.37, -0.64, 0.15, -0.62, -0.36, -0.12, 0.78, 0.45, 0.19, -0.20, -0.16, -0.08, -0.27, 0.39)$, $(v_1, \cdots, v_{14}) = (-0.55, -0.45, -0.35, -0.25, -0.15, -0.05, 0.1, 0.2, 0.3, 0.4, 0.5, 0.6, 0.7, 0.8)$. The number of sensors considered in this example is $L = 11$. The SNR and the number of snapshots are fixed at 30 dB and $N = 1000$, respectively. Fig. 6 shows the direction-cosine estimation results for ten independent trials. It is seen from the figure that the proposed algorithm successfully resolves the 14 sources, as stated in Section III.B: $M = 2(L - 4)$.

In the last example, we compare the computational complexities of different algorithms. Fig. 7 shows the multiplications required by the five algorithms as a function of the number of snapshots. The number of sensors considered is $L = 11$, and the number sources is set as $M = 2$. It is seen from the figure that the proposed algorithm is computationally more complex than the other four algorithms.

V. CONCLUSION

A new cumulant based algorithm is proposed in this paper to estimate 2D arrival angles of multiple narrowband non-Gaussian signals. In the proposed algorithm, we present an array geometry consisting of a nine-element non-uniformly spaced cross-shaped sub-array plus another arbitrarily-spaced sub-array to define five cumulant matrices, from which the signal direction cosines can be estimated by using PARAFAC fitting. The proposed algorithm achieves array aperture extension by jointly extending array physical aperture and constructing virtual sensors, and requires no open-form two-dimensional searching and parameter pairing. In addition, it can resolve $2(L - 4)$ signals with an array of L sensors. Incidently, as the fourth-order cumulant can naturally suppress the correlated noise, the proposed algorithm would be robust in the presence of spatially correlated noise.

REFERENCES

[1] R. O. Schmidt, "Multiple emitter location and signal parameter estimation," *IEEE Trans. Antennas Propag.*, vol. AP-34, no. 3, pp. 276–280, Mar. 1986.

[2] R. Roy and T. Kailath, "Esprit-estimation of signal parameters via rotational invariance techniques," *IEEE Trans. Acoust., Speech, Signal Process.*, vol. 37, no. 7, pp. 984–995, Jul. 1989.

[3] A. Y. J. Chan and J. Litva, "MUSIC and maximum likelihood techniques on two-dimensional DOA estimation with uniform circular array," *IEE Proc.–Radar, Sonar Navigat.*, vol. 142, no. 3, pp. 105–114, Jun. 1995.

[4] C. P. Mathews and M. D. Zoltowski, "Eigenstructure techniques for 2-D angle estimation with uniform circular arrays," *IEEE Trans. Signal Process.*, vol. 42, no. 9, pp. 2395–2407, Sep. 1994.

[5] X. Yang, G. Li, Z. Zheng, and L. Zhong, "2D DOA estimation of coherently distributed noncircular sources," *Wireless Pers. Commun.*, vol. 78, no. 2, pp. 1095–1102, 2014.

[6] P. Vallet *et al.*, "Performance analysis of an improved music DOA estimator," *IEEE Trans. Signal Process.*, vol. 63, no. 23, pp. 6407–6422, Dec. 2015.

[7] X. Lan, Y. Li, and E. Wang, "A rare algorithm for 2D DOA estimation based on nested array in massive MIMO system," *IEEE ACCESS*, vol. 4, pp. 3806–3814, Aug. 2016.

[8] D. Zhang, Y. Zhang, G. Zheng, B. Deng, C. Feng, and J. Tang, "Two-dimensional direction of arrival estimation for coprime planar arrays via polynomial root finding technique," *IEEE Access*, vol. 6, pp. 19540–19549, 2018, doi: 10.1109/ACCESS.2018.2821919.

[9] J. E. F. del Rio and M. F. Catedra-Peraz, "The matrix pencil method for two-dimensional direction of arrival estimation employing an L-shaped array," *IEEE Trans. Antennas Propag.*, vol. 45, no. 11, pp. 1693–1694, Nov. 1997.

[10] N. Tayem and H. M. Kwon, "L-shape 2-dimensional arrival angle estimation with propagator method," *IEEE Trans. Antennas Propag.*, vol. 53, no. 5, pp. 1622–1630, May 2005.

[11] Y. Wu, G. Liao, and H.-C. So, "A fast algorithm for 2-D direction-of-arrival estimation," *Signal Process.*, vol. 83, no. 8, pp. 1827–1831, 2003.

[12] H. Shao, W. Su, H. Gu, J. Fan, and J. Chen, "Virtual matrix pencil method for 2-D DOA estimation with a two-nested-shape-array," *Multidimensional Syst. Signal Process.*, vol. 26, no. 3, pp. 619–644, 2015.

[13] N. Tayem *et al.*, "Two-dimensional DOA estimation using cross-correlation matrix with L-shaped array," *IEEE Antennas Wireless Propag. Lett.*, vol. 15, pp. 1077–1080, Mar. 2016.

[14] B. Li, W. Bai, Q. Zhang, G. Zheng, J. Bai, and X. Fu, "High accuracy and unambiguous 2D-DOA estimation with an uniform planar array of 'Long' electric-dipoles," *IEEE Access*, vol. 6, pp. 40559–40568, 2018.
[15] A. J. van der Veen, P. B. Ober, and E. F. Deprettere, "Azimuth and elevation computation in high resolution DOA estimation," *IEEE Trans. Signal Process.*, vol. 40, no. 7, pp. 1828–1832, Jul. 1992.
[16] S. Kikuchi, H. Tsuji, and A. Sano, "Pair-matching method for estimating 2-D angle of arrival with a cross-correlation matrix," *IEEE Antennas Wireless Propag. Lett.*, vol. 5, pp. 35–40, 2006.
[17] J.-F. Gu and P. Wei, "Joint SVD of two cross-correlation matrices to achieve automatic pairing in 2-D angle estimation problems," *IEEE Antennas Wireless Propag. Lett.*, vol. 6, pp. 553–556, 2007.
[18] Q. Y. Yin, R. W. Newcomb, and L. H. Zou, "Estimating 2-D angles of arrival via two parallel linear arrays," in *Proc. Int. Conf. Acoust., Speech, Signal Process. (ICASSP)*, vol. 4, May 1989, pp. 2803–2806.
[19] F. A. Sakarya and M. W. Hayes, "Estimating 2-D DOA angles using nonlinear array configurations," *IEEE Trans. Signal Process.*, vol. 43, no. 9, pp. 2212–2216, Sep. 1995.
[20] K. T. Wong and M. D. Zoltowski, "Extended-aperture underwater acoustic multisource azimuth/elevation direction-finding using uniformly but sparsely spaced vector hydrophones," *IEEE J. Ocean. Eng.*, vol. 22, no. 4, pp. 659–672, Oct. 1997.
[21] K. T. Wong and M. D. Zoltowski, "Direction-finding with sparse rectangular dual-size spatial invariance array," *IEEE Trans. Aerosp. Electron. Syst.*, vol. 34, no. 4, pp. 1320–1336, Oct. 1998.
[22] M. D. Zoltowski and K. T. Wong, "ESPRIT-based 2-D direction finding with a sparse uniform array of electromagnetic vector sensors," *IEEE Trans. Signal Process.*, vol. 48, no. 8, pp. 2195–2204, Aug. 2000.
[23] M. D. Zoltowski and K. T. Wong, "Closed-form eigenstructure-based direction finding using arbitrary but identical subarrays on a sparse uniform Cartesian array grid," *IEEE Trans. Signal Process.*, vol. 48, no. 8, pp. 2205–2210, Aug. 2000.
[24] J. He and Z. Liu, "Extended aperture 2-D direction finding with a two-parallel-shape-array using propagator method," *IEEE Antennas Wireless Propag. Lett.*, vol. 8, pp. 323–327, 2009.
[25] S. Miron, Y. Song, D. Brie, and K. T. Wong, "Multilinear direction finding for sensor-array with multiple scales of invariance," *IEEE Trans. Aerosp. Electron. Syst.*, vol. 51, no. 3, pp. 2057–2070, Jul. 2015.
[26] T.-H. Liu and J. M. Mendel, "Azimuth and elevation direction finding using arbitrary array geometries," *IEEE Trans. Signal Process.*, vol. 46, no. 7, pp. 2061–2065, Jul. 1998.
[27] P. Chevalier, A. Ferréol, and L. Albera, "High-resolution direction finding from higher order statistics: The 2q-MUSIC algorithm," *IEEE Trans. Signal Process.*, vol. 54, no. 8, pp. 2986–2997, Aug. 2006.
[28] J. Liang, "Joint azimuth and elevation direction finding using cumulant," *IEEE Sensors J.*, vol. 9, no. 4, pp. 390–398, Apr. 2009.
[29] N. D. Sidiropoulos, G. B. Giannakis, and R. Bro, "Blind PARAFAC receivers for DS-CDMA systems," *IEEE Trans. Signal Process.*, vol. 48, no. 3, pp. 810–823, Mar. 2000.
[30] N. D. Sidiropoulos, R. Bro, and G. B. Giannakis, "Parallel factor analysis in sensor array processing," *IEEE Trans. Signal Process.*, vol. 48, no. 8, pp. 2377–2388, Aug. 2000.
[31] R. A. Harshman, "Foundations of the PARAFAC procedure: Models and conditions for an 'explanatory' multi-modal factor analysis," *UCLA Working Papers Phonetics*, vol. 16, pp. 1–84, Dec. 1970.
[32] J. D. Carroll and J.-J. Chang, "Analysis of individual differences in multidimensional scaling via an n-way generalization of 'Eckart-Young' decomposition," *Psychometrika*, vol. 35, no. 3, pp. 283–319, 1970.
[33] J. M. Mendel, "Tutorial on higher-order statistics (spectra) in signal processing and system theory: Theoretical results and some applications," *Proc. IEEE*, vol. 79, no. 3, pp. 278–305, Mar. 1991.
[34] J. B. Kruskal, "Three-way arrays: Rank and uniqueness of trilinear decompositions, with application to arithmetic complexity and statistics," *Linear Algebra Appl.*, vol. 18, no. 2, pp. 95–138, 1975.
[35] Y. Rong, S. A. Vorobyov, A. B. Gershman, and N. D. Sidiropoulos, "Blind spatial signature estimation via time-varying user power loading and parallel factor analysis," *IEEE Trans. Signal Process.*, vol. 53, no. 5, pp. 1697–1710, May 2005.

CHEN GU received the Ph.D. degree in communication and information system from the Nanjing University of Science and Technology, Nanjing, China, in 2010. Since 2010, she has been a Lecturer with the Nanjing University of Science and Technology. Her current research interests include radar signal analysis and processing, array signal processing, and noncontact vital signs monitoring.

HONG HONG (M'10) received the Ph.D. degree in electrical engineering from Nanjing University, Nanjing, China, in 2010. Since 2010, he has been a Lecturer with the Nanjing University of Science and Technology, Nanjing. In 2014, he was a Visiting Scholar with the Institute of Biomedical Engineering and Technology, Sydney University, Sydney, NSW, Australia. His current research interests include biomedical radar applications of microwave and RF circuits and systems, speech signal processing, and radar signal processing.

XIAOHUA ZHU received the Ph.D. degree in communication and information system from the Nanjing University of Science and Technology, Nanjing, China, in 2002. He is currently a Professor with the School of Electronic and Optical Engineering, Nanjing University of Science and Technology. He is also the Leader of the Radar and High-speed Digital Signal Processing Laboratory, Nanjing University of Science and Technology. He has authored or co-authored four books, and more than 100 papers. He has submitted 18 patent applications. His current research interests include radar system, radar signal theory, and digital signal processing. He received the Ministerial and Provincial-Level Science and Technology Award ten times.

JIN HE received the B.S. degree in information engineering from Tongji University, Shanghai, China, in 2001, and the M.S. and Ph.D. degrees in electrical engineering from the Nanjing University of Science and Technology (NJUST), Nanjing, Jiangsu, China, in 2004 and 2007, respectively. From 2007 to 2009, he was a Post-Doctoral Fellow with the Department of Electrical Engineering, NJUST, where he was the Program Director and was responsible for the China Postdoctoral Science Projects. From 2009 to 2011, he was a Post-Doctoral Fellow with the Department of Electrical and Computer Engineering, Concordia University, Montreal, QC, Canada. From 2012 to 2015, he was a Research Engineer with the Shanghai Aerospace Electronic Technology Institute, Shanghai, China. He is currently an Associate Professor with the Shanghai Key Laboratory of Intelligent Sensing and Recognition, Department of Electronic Engineering, Shanghai Jiaotong University, Shanghai. His research interests include array signal processing, statistical signal processing, non-Gaussian signal processing, and their applications. Also, he has served as a peer-reviewer for various IEEE/IET research journals since 2007.